HHS Public Access

Author manuscript

ACS Appl Mater Interfaces. Author manuscript; available in PMC 2018 April 25.

Published in final edited form as:

ACS Appl Mater Interfaces. 2017 December 06; 9(48): 41700–41711. doi:10.1021/acsami.7b14083.

CuS-Based Theranostic Micelles for NIR-Controlled Combination Chemotherapy and Photothermal Therapy and Photoacoustic Imaging

Guojun Chen[†,‡,#], **Ben Ma**[‡,||,#], **Yuyuan Wang**[†,‡], **Ruosen Xie**[†,‡], **Chun Li**[⊥], **Kefeng Dou**[||,*], and **Shaoqin Gong**[†,§,*]

[†]Department of Materials Science and Engineering, University of Wisconsin—Madison, Madison, Wisconsin 53715, United States

[‡]Wisconsin Institute for Discovery and Department of Biomedical Engineering, University of Wisconsin—Madison, Madison, Wisconsin 53715, United States

[§]Department of Chemistry, University of Wisconsin—Madison, Madison, Wisconsin 53715, United States

[||]Department of Hepatobiliary Surgery, Xijing Hospital, Fourth Military Medical University, Xi'an, Shaanxi 710032, China

[⊥]Department of Cancer Systems Imaging, The University of Texas MD Anderson Cancer Center, Houston, Texas 77054, United States

Abstract

Cancer remains a major threat to human health due to low therapeutic efficacies of currently available cancer treatment options. Nanotheranostics, capable of simultaneous therapy and diagnosis/monitoring of diseases, has attracted increasing amounts of attention, particularly for cancer treatment. In this study, CuS-based theranostic micelles capable of simultaneous combination chemotherapy and photothermal therapy (PTT), as well as photoacoustic imaging, were developed for targeted cancer therapy. The micelle was formed by a CuS nanoparticle (NP) functionalized by thermosensitive amphiphilic poly(acrylamide-acrylonitrile)–poly(ethylene glycol) block copolymers. CuS NPs under near-infrared (NIR) irradiation induced a significant temperature elevation, thereby enabling NIR-triggered PTT. Moreover, the hydrophobic core formed by poly(acrylamide-acrylonitrile) segments used for drug encapsulation exhibited an upper critical solution temperature (UCST; ~38 °C), which underwent a hydrophobic-to-hydrophilic

[*]Corresponding Authors: shaoqingong@wisc.edu (S.G.). doukef@fmmu.edu.cn (K.D.).

[#]**Author Contributions**

G.C. and B.M. contributed equally.

ORCID

Chun Li: 0000-0002-2376-4703

Shaoqin Gong: 0000-0001-9447-2938

Notes

The authors declare no competing financial interest.

Supporting Information

The Supporting Information is available free of charge on the ACS Publications website at DOI: 10.1021/acsami.7b14083. MCTS formation using hanging drop method; FTIR spectra of polymers; temperature–transmission profile, DLS analyses of CuS-based micelles; cell viability test; micelle distribution in MCTS; AF-loading level calculation (PDF)

transition once the temperature rose above the UCST induced by NIR-irradiated CuS NPs, thereby triggering a rapid drug release and enabling NIR-controlled chemotherapy. The CuS-based micelles conjugated with GE11 peptides were tested in an epidermal growth factor receptor-overexpressing triple-negative breast cancer model. In both two-dimensional monolayer cell and three-dimensional multicellular tumor spheroid models, GE11-tagged CuS-based micelles under NIR irradiation, enabling the combination chemotherapy and PTT, exhibited the best therapeutic outcome due to a synergistic effect. These CuS-based micelles also displayed a good photoacoustic imaging ability under NIR illumination. Taken together, this multifunctional CuS-based micelle could be a promising nanoplatform for targeted cancer nanotheranostics.

Graphical Abstract

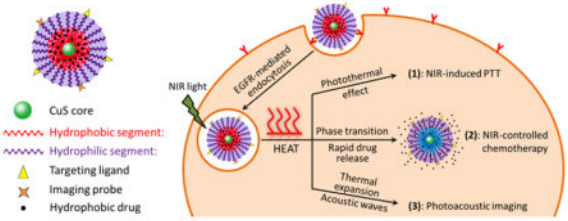

Keywords

nanotheranostics; combination therapy; CuS NPs; NIR-controlled drug release; photothermal therapy; photoacoustic imaging; thermoresponsive micelle

1. INTRODUCTION

Despite years of intense efforts on cancer research, cancer remains one of the greatest threats to human health, causing millions of deaths every year.[1,2] Existing cancer treatment modalities, including chemotherapy, surgical resection, and radiotherapy, still suffer from many drawbacks, including drug resistance, severe toxic side effects, incomplete tumor elimination, disease recurrence, and lesion development on irradiated tissues.[2–5] Thus, innovative cancer treatment strategies with high tumor specificity and high therapeutic efficacy, yet low systemic toxicity, are still in great demand.

Cancer nanotheranostics, capable of combined cancer treatment and cancer diagnosis/monitoring using a single nanomedicine, has recently attracted intense attention due to the various advantages it can offer.[6–8] First, in contrast to standard chemotherapy that lacks tumor-targeting ability, drug nanocarriers possess both passive and active tumor-targeting abilities.[9–11] Considerable progress in the design and development of intelligent drug nanocarriers has been made in recent years, which can improve therapeutic efficacies and minimize side effects.[12–14] Second, cancer nanotheranostics can enable cancer diagnosis and/or monitoring of treatment efficacy through various imaging modalities.[15–17] Enhanced tumor imaging/monitoring enabled by drug nanocarriers can be achieved by either attaching different imaging moieties (e.g., dyes for optical imaging, radioisotopes for positron-emission tomography, and contrast agents for magnetic resonance imaging (MRI)) to the nanocarriers or by taking advantage of the intrinsic imaging properties of certain

nanoparticles (NPs) (e.g., superparamagnetic iron oxide for MRI, CuS NPs for photoacoustic (PA) imaging, and quantum dots for optical imaging).[15–19] Theranostic NPs allow physicians to monitor tumor sizes, locations, and possible metastases in real time throughout the entire treatment process, thereby making it possible to readily adjust the therapeutic regimen in a timely manner.[6,20] Finally, yet critically importantly, NPs can deliver multiple payloads simultaneously for combination therapy. Combination therapy, such as targeted chemotherapy and photothermal therapy (PTT), can significantly enhance antitumor efficacy.[21–23]

Owing to its high specificity, high treatment efficacy, and low side effects, photothermal therapy (PTT) has attracted tremendous attention as an alternative cancer treatment strategy in recent years.[24,25] It employs photothermal conversion agents, which can strongly absorb light and convert photon energy to local heating, for cancerous cell killing or ablation.[24,25] Importantly, NP-mediated hyperthermia can be directed at the tumor site in an on-demand manner and the temperature elevation can be easily tuned by controlling the time and intensity of the extrinsic lights. Of particular interest, near-infrared (NIR)-light-induced photothermal therapy (PTT) is highly desirable due to its high tissue penetration depth.[24–26] Numerous photothermal coupling agents, especially nanoparticles with strong absorbance in the NIR region, have been investigated to achieve high photothermal conversion efficiency.[25] Among them, CuS NPs have attracted particular attention because of their low cost, low cytotoxicity, and high photothermal conversion efficiency.[27,28] In addition, CuS NPs intrinsically possess PA imaging properties.[29] PA imaging, based on the photoacoustic effect, is an imaging modality that utilizes the high contrast of optical imaging and deep tissue penetration ability of ultrasound.[30] Therefore, CuS-based drug nanocarriers may be suitable for targeted cancer nanotheranostics.

In this study, we have designed a unique CuS-based theranostic micelle for combination chemotherapy and PTT, as well as PA imaging. As shown in Figure 1, an individual CuS NP was functionalized with thermosensitive amphiphilic block copolymers, namely, poly(acrylamide-acrylonitrile)–poly-(ethylene glycol) (PAAmAN–PEG), to form the CuS-based theranostic micelle. The hydrophobic segment, PAAmAN, was designed to encapsulate hydrophobic drugs (e.g., aminoflavone (AF) in this study). PAAmAN is one of the few thermosensitive polymers that exhibit an upper critical solution temperature (UCST) in water.[31] The UCST of PAAmAN designed in this study was slightly higher than human body temperature, thus avoiding a burst release of drugs under normal physiological conditions. Once the temperature reaches the UCST of PAAmAN polymers, hydrophobic-to-hydrophilic phase transition occurs, subsequently inducing a rapid release of the encapsulated hydrophobic drug (Figure 2). We and others have previously demonstrated that a rapid release of anticancer drugs within the tumor sites can lead to superior anticancer efficacies.[32–35] In this work, the temperature elevation generated by the CuS NP core under NIR light induced both the PTT effect and the hydrophobic-to-hydrophilic phase transition of PAAmAN, leading to a rapid drug release, thereby achieving NIR-controlled combination chemotherapy and PTT. We tested these CuS-based micelles in triple-negative breast cancer (TNBC) models. The GE11 peptide, which binds efficiently to the epidermal growth factor receptor (EGFR) overexpressed by TNBCs, was used as an active tumor-targeting ligand.[12,36] Our results demonstrated that in both two-dimensional (2D) monolayer cell and three-

dimensional (3D) multicellular tumor spheroid (MCTS) models, GE11-conjugated CuS-based micelles under NIR irradiation, enabling TNBC-targeted combination chemotherapy and PTT, exhibited a significantly better therapeutic outcome compared to that of chemotherapy alone or PTT alone. We have also shown that this CuS-based micelle could effectively serve as a PA imaging probe under NIR illumination.

2. MATERIALS AND METHODS

2.1. Materials

Copper bromide ($CuBr_2$), sodium sulfide (Na_2S), dimethyl sulfoxide (DMSO), and 4-cyano-4-(phenylcarbonothioylthio) pentanoic acid *N*-succinimidyl ester (CPPA-NHS) were purchased from Sigma-Aldrich (St. Louis, MO). Acrylamide (AAm), acrylonitrile (AN), azobisisobutyronitrile (AIBN), Traut's agent, and tris(2-carboxyethyl)phosphine (TECP) were obtained from Thermo Fisher Scientific (Fitchburg, WI). Cy5 was purchased from Lumiprobe Corporation (Hallandale Beach, FL). GE11 peptide (amino acid sequence: YHWYGYTPQNVIGGGGC) was purchased from Tufts University Core Facility (Boston, MA). AF was obtained from the Developmental Therapeutics Program Repository of the National Cancer Institute at Frederick (Frederick, MD). Other Reagents were purchased from Thermo Fisher Scientific (Fitchburg, WI).

2.2. Synthesis of AF-Loaded GE11-Conjugated CuS-Based Micelles

2.2.1. Synthesis of CuS-COOH NPs—Copper bromide ($CuBr_2$; 10 mL, 1.41 mg/mL) and sodium citrate (10 mL, 1.0 mg/mL) water solutions were added into deionized (DI) water (30 mL). The mixture was stirred at room temperature for 30 min before the addition of a Na_2S (50 μL, 60.54 mg/250 μL) solution. Thereafter, the solution was stirred for another 5 min and transferred to a 90 °C water bath. The reaction was maintained for 15 min and was subsequently cooled down with ice. A green-colored CuS-COOH NP solution was obtained.

2.2.2. Synthesis of Maleimide-Functionalized CuS NPs (i.e., CuS-Mal NPs)—*N*-(2-Aminoethyl)maleimide (1.2 mg), 1-ethyl-3-(3-dimethylaminopropyl)carbodiimide (1.3 mg), and *N*-hydroxysuccini-mide (1.5 mg) were added to the CuS-COOH NP solution (5 mL, 1 mg/mL). The reaction was carried out for 48 h, and impurities were removed by dialysis against DI water for 48 h. The final product was dried under lyophilization.

2.2.3. Synthesis of Mal-PEG-(4-Cyano-4-(phenylcarbonothioylthio)pentanoic acid) (i.e., Mal-PEG-CPPA) Reversible Addition Fragmentation Chain Transfer (RAFT) Macro-initiator—Mal-PEG-NH_2 (10 mg) and CPPA-NHS (2 mg) RAFT agent were dissolved in dimethylformamide (DMF, 3 mL). The reaction was carried out at room temperature in the dark overnight, and the solution was then added dropwise into cold diethyl ether to get the crude product. The resulting product (i.e., Mal-PEG-CPPA) was purified through a precipitation process repeated three times. The final polymer was dried under vacuum. mPEG-CPPA was prepared following a similar method using mPEG-NH_2 instead. The chemical structures of Mal-PEG-CPPA and mPEG-CPPA were confirmed by ^{1}H NMR (Bruker Advanced 400, 400 MHz, $CDCl_3$). Mal-PEG-CPPA: δ 1.25 (6H, s), 1.97

(2H, t), 2.26 (2H, t), 3.21 (3H, s), 3.4–3.67 (453H, m), 6.67 (2H, d), 7.36–7.47 (3H, d), and 7.74 (2H, d). mPEG-CPPA: δ 1.25 (6H, s), 1.97 (2H, t), 2.26 (2H, t), 3.21 (3H, s), 3.40–3.67 (454H, m), 7.40 (3H, d), and 7.74 (2H, d).

2.2.4. Synthesis of Mal-PEG-Poly(acrylamide-acrylonitrile) (i.e., Mal-PEG-PAAmAN)—Mal-PEG-CPPA (20 mg), AAm (22.1 mg), AN (10.2 mg), and AIBN (0.321 mg) were dissolved in DMF (0.3 mL). After complete degasification by a standard freeze–pump–thaw cycling process, the vial was sealed under vacuum and placed into an 80 °C oil bath to begin the polymerization process. After 24 h, the resulting solution was added dropwise into cold diethyl ether to obtain the crude products, which were further purified by a precipitation process repeated three times. The final polymer was dried under vacuum. mPEG-PAAmAN was prepared following a similar method using mPEG-CPPA as the macroinitiator. The chemical structures of Mal-PEG-PAAmAN and mPEG-PAAmAN were confirmed by ^{1}H NMR (DMSO-d_6). Mal-PEG-PAAmAN: δ 0.98 (6H, m), 1.46–1.83 (63H, m), 2.57 (26H, m), 2.9 (4H, m), 3.4–3.67 (452H, m), 6.67 (2H, d), 7.36–7.47 (3H, d), and 7.74 (2H, d). mPEG-PAAmAN: δ 0.98 (6H, m), 1.46–1.83 (61H, m), 2.57 (25H, m), 2.9 (4H, m), 3.4–3.67 (451H, m), 7.36–7.47 (3H, d), and 7.74 (2H, d).

2.2.5. Synthesis of GE11 (or Cy5)-PEG-PAAmAN—Mal-PEG-PAAmAN (20 mg), GE11 (0.2 mg), and TECP (0.1 mg) were dissolved in DMF (3 mL). The reaction was carried out for 24 h at room temperature. Impurities were removed by dialysis against DI water for 48 h. The final polymer was freeze-dried. Cy5-PEG-PAAmAN was prepared following a similar method using Cy5-SH instead. The chemical structures of GE11-PEG-PAAmAN and Cy5-PEG-PAAmAN were confirmed by ^{1}H NMR (DMSO-d_6). GE11-PEG-PAAmAN: δ 0.98 (6H, m), 1.46–1.83 (63H, m), 2.57 (26H, m), 2.9 (4H, m), 3.4–3.67 (452H, m), 6.67 (2H, d), and 7.1–7.7 (62H, d). Cy5-PEG-PAAmAN: δ 0.98 (6H, m), 1.46–1.83 (63H, m), 2.57 (26H, m), 2.9 (4H, m), 3.4–3.67 (452H, m), 6.67 (2H, m), and 7.1–7.8 (25H, m).

2.2.6. Synthesis of GE11 (or Cy5, or OCH_3)-PEG-PAAmAN-SH—GE11-PEG-PAAmAN (20 mg) and hexylamine (2.3 mg) were dissolved in DMF (5 mL). The hydrazinolysis started immediately, indicated by a rapid fading of the pink color of the solution.[37] The hydrazinolysis was allowed to continue for 12 h at room temperature. The resulting solution was dialyzed against DI water for 48 h to remove impurities. The final product was dried under lyophilization. Cy5-PEG-PAAmAN-SH or mPEG-PAAmAN-SH was prepared following a similar method using Cy5-PEG-PAAmAN or mPEG-PAAmAN, respectively, instead. The chemical structures of GE11-PEG-PAAmAN-SH, Cy5-PEG-PAAmAN-SH, and mPEG-PAAmAN-SH were confirmed by ^{1}H NMR (DMSO-d_6). GE11-PEG-PAAmAN-SH: δ 0.98 (6H, m), 1.46–1.83 (63H, m), 2.57 (26H, m), 2.9 (4H, m), 3.4–3.67 (452H, m), 6.67 (2H, d), and 7.1–7.7 (55H, d). Cy5-PEG-PAAmAN-SH: δ 0.98 (6H, m), 1.46–1.83 (63H, m), 2.57 (26H, m), 2.9 (4H, m), 3.4–3.67 (452H, m), 6.67 (2H, m), and 7.1–7.8 (20H, m). mPEG-PAAmAN-SH: δ 0.98 (6H, m), 1.46–1.83 (61H, m), 2.57 (25H, m), 2.9 (4H, m), and 3.4–3.67 (451H, m).

2.2.7. Synthesis of CuS-PAAmAN-PEG—To prepare CuS-PAAmAN-PEG-GE11/Cy5/OCH_3, CuS-Mal NPs (5 mg), Cy5.5-PEG-PAAmAN-SH (3.1 mg), GE11-PAAmAN-SH (6.2 mg), and mPEG-PAAmAN-SH (53.1 mg) were dissolved in DMSO (5 mL) in the presence of TCEP (2.1 mg). The reaction was carried out for 48 h, and impurities were removed by dialysis against DMF for 24 h and DI water for another 24 h. The final product was dried under lyophilization. CuS-PAAmAN-PEG-Cy5/OCH_3, CuS-PAAmAN-PEG-GE11/OCH_3, and CuS-PAAmAN-PEG-OCH_3 were prepared following a similar method.

2.2.8. Synthesis of AF-Loaded CuS-Based Micelles—To prepare AF-loaded targeted CuS-based micelles, AF (15 mg) and CuS-PAAmAN-PEG-GE11/OCH_3 (60 mg) were dissolved in DMSO (3 mL). DI water (9 mL) was added dropwise into the solution. After stirring for another 2 h, the solution was dialyzed against DI water for 48 h. The final product was obtained after lyophilization.

2.3. Characterizations

Molecular weights (M_n and M_w) and polydispersity indices (PDIs) of all polymers were measured using a gel permeation chromatography (Viscotek) instrument equipped with triple detectors, including a refractive index detector, a viscometer detector, and a light scattering detector. The morphologies of the micelles were studied by transmission electron microscopy (TEM, FEI Tecnai G^2 F30 TWIN 300 kV, E.A. Fischione Instruments, Inc.) and dynamic light scattering (DLS, ZetaSizer Nano ZS90, Malvern Instruments). The AF loading level (i.e., the weight percentage of AF in AF-loaded micelles) was determined by UV–vis spectrometry (Varian Cary 300 Bio UV–vis spectrophotometer, Agilent Technologies, Santa Clara, CA) at 357 nm. The temperature-dependent phase transition of CuS-based micelles was determined by measuring their optical transmittances in an aqueous solution (3 mg/mL) at 670 nm at various temperatures using a UV–vis spectrophotometer.[38]

2.4. NIR-Light-Induced Photothermal Effect of CuS-Based Micelle Solution

To study the photothermal effect of CuS-based micelles, CuS-based micelle solutions with different concentrations (10–60 μg/mL) were illuminated by a 980 nm laser at a power density of 0.75 W/cm^2 for 5 min. The temperature changes of the solutions were monitored with a digital thermometer throughout the experiments.

2.5. NIR-Light-Triggered in Vitro Drug Release

The AF-loaded CuS-based micelle solution (1 mL; 1 mg/mL) was placed in a dialysis tube (molecular weight cutoff, 8 kDa), which was then immersed in 15 mL of phosphate-buffered saline (PBS) (pH 7.4) or acetate buffer solution (pH 5.3). After 6 h incubation, the samples were irradiated with a 980 nm laser at an output power of 0.75 W/cm^2 over a period of 10 min. At certain time points, 3 mL of release media was collected and replaced by an equal amount of fresh media. The drug release behavior was monitored for 48 h. Amounts of AF in the collected media were quantified by a UV–vis spectrophotometer at 357 nm. Samples kept in the dark (i.e., without 980 nm irradiation) throughout the experiment were also analyzed.

2.6. Cellular Uptake Studies in a 2D Monolayer Cell Model

MDA-MB-468 cells were cultured in Dulbecco's modified Eagle's medium (Gibco, Gaithersburg, MD) containing 10% fetal bovine serum (Gibco, Gaithersburg, MD) and 1% penicillin/streptomycin (Thermo Fisher, Fitchburg, WI) under standard conditions (37 °C/5% CO_2/95% humidity). Cellular uptake of the micelles was examined using flow cytometry and fluorescence microscopy based on the fluorescence of Cy5 fluorophore tagged onto the micelles. For the flow cytometry study, MDA-MB-468 cells were seeded in 24-well plates (1×10^5 cells per well) and cultured for 24 h before use. Cells were then treated with culture medium (control), nontargeted (NT) CuS-based micelles (i.e., without GE11 conjugation), targeted CuS-based micelles (i.e., with GE11 conjugation), or targeted CuS-based micelles with free GE11 peptide (2 μM; i.e., the competitive binding or blocking assay) at a micelle concentration of 100 μg/mL. After incubation for 2 h, cells were washed with PBS three times and harvested with 0.25% ethylenediaminetetraacetic acid–trypsin (Gibco, Gaithersburg, MD). Cells were then collected by centrifugation at a speed of 130*g* for 5 min and resuspended in 600 μL of PBS for testing. Data were acquired with an Attune NxT flow cytometer (Thermo Fisher, Fitchburg, WI) and analyzed with FlowJo 7.6 (Ashland, OR). For fluorescence microscopy studies, cells were seeded in 24-well plates and cultured for 24 h before use. Cells were then treated the same way as described for the flow cytometry studies. After 2 h incubation, cells were washed with PBS three times and fixed with 4% paraformaldehyde. Cell nuclei were stained with Hoechst 33342 (Thermo Fisher, Fitchburg, WI). Cells were then imaged under a fluorescence microscope (Nikon, Japan).

2.7. Cell Viability Studies in a 2D Monolayer Cell Model

MDA-MB-468 cells were seeded in 96-well plates (15000 cells per well) and cultured for 24 h before use. Cells were treated with various formulations as summarized in Table 1 with an AF concentration of 0.05 μg/mL. After 6 h incubation, cells were irradiated by a 980 nm laser (0.75 W/cm^2, 10 min). Thereafter, cells were incubated for another 18 h before introducing 3-(4,5-dimethylthiazol-2-yl)-2,5-diphenyltetrazolium bromide (MTT) agents (Sigma-Aldrich, St. Louis, MO). For comparison purposes, cells were treated with the same formulations shown in Table 1 but without laser treatment. Finally, the cell viabilities (percentage of the control group without 980 nm laser application) were determined using a standard MTT assay.[17]

2.8. Preparation of the MDA-MB-468 3D Multicellular Tumor Spheroid (MCTS) Culture Model

An MDA-MB-468 MCTS 3D culture model was formed using the hanging drop method[39,40] as illustrated in Figure S1 (Supporting Information). Briefly, MDA-MB-468 cells were suspended in complete growth medium containing 0.24% (v/v) methylcellulose (50 cell/μL). The drops of the cell suspension (20 μL/drop) were deposited onto a 96-well plate (low attachment; Corning, NY), which was then inverted onto a lid with PBS drops (10 μL/drop). After incubation for 5 days under standard cell culture conditions (37 °C/5% CO_2/95% humidity), cells in the hanging drops aggregated at the medium/air interface and formed MCTSs with a size of around 500 μm. The 96-well plates were then turned over and filled with 100 μL of complete growth medium per well.

2.9. Micelle Penetration Studies in a 3D Culture Model

MDA-MB-468 MCTSs were treated with Cy5-tagged nontargeted and targeted CuS-based micelles with a micelle concentration of 100 μg/mL. After certain time points (i.e., 2, 6, and 24 h), MCTSs were washed gently with PBS and the nuclei were stained with Hoechst 33342. Samples were then analyzed using a confocal laser scanning microscope.

2.10. Cell Viability Studies in a 3D Culture Model

Cell viabilities in MCTS were determined by MTT and PI/annexin-V assays. MCTSs were treated with various conditions as summarized in Table 1 with an AF concentration of 0.05 μg/mL. After 6 h incubation, MCTSs were irradiated by a 980 nm laser at a power density of 0.75 W/cm^2 for 10 min and were then incubated for another 18 h. For comparison, MCTSs were treated with the same formulations for 24 h, but without laser irradiation. Finally, cell viability in the MCTS 3D model (percentage of the control group without 980 nm laser illumination) was determined using a standard MTT assay or PI/annexin-V assay (Thermo Fisher, Fitchburg, WI) following the manufacturer's protocols.

2.11. In Vitro Photoacoustic Imaging

To investigate the photoacoustic imaging capabilities of CuS-based micelles, CuS-based micelle solutions of various concentrations (0.05, 0.1, 0.25, and 0.5 mg/mL) were prepared and analyzed using a VEVO LASR PA imaging system (VisualSonics, Inc., Toronto, Canada). The PA images were collected at a laser excitation wavelength of 970 nm, with a 21 MHz transducer in both B mode and PA mode at 18 and 53 dB gains, respectively.

3. RESULTS AND DISCUSSION

3.1. Synthesis and Characterization of CuS-Based Theranostic Micelles

Carboxyl-capped CuS (i.e., CuS-COOH) NPs were first synthesized in an aqueous solution by reacting $CuBr_2$ and Na_2S in the presence of sodium citrate. The ζ potential of the CuS-COOH NPs was −23 mV, demonstrating the presence of carboxyl (–COOH) groups on the surface of the CuS NPs.[27] The carboxyl (–COOH) surface groups were then converted to maleimide (Mal) groups in the presence of *N*-(2-aminoethyl)maleimide through amidization to generate CuS-Mal NPs, which was confirmed by the Fourier transform infrared (FTIR) spectrum shown in Figure S2. The average size of the CuS-Mal NPs was 8.9 nm (PDI = 0.15), as measured by DLS (Figure 3A). Figure 3B shows a representative TEM image of the CuS-Mal NPs. The CuS NPs were well-dispersed in water and relatively uniform in size. Figure 3C shows the UV–vis–NIR absorption spectrum of the CuS-Mal NPs in water. A strong absorption band in the NIR region was observed with a peak at 989 nm. The strong NIR absorption capability exhibited by the CuS NPs makes them a suitable candidate for NIR-induced PTT and NIR-controlled drug release through thermally induced phase transition, as discussed below.

Thermoresponsive amphiphilic block copolymer PAAmAN–PEG was synthesized via reversible addition fragmentation chain transfer (RAFT) polymerization, as shown in Scheme 1. The CPPA terminals were then converted to–SH groups via hydrazinolysis.[37] Thereafter, SH-PAAmAN-PEGs were conjugated onto the CuS-Mal NPs via Mal-SH click

chemistry. FTIR spectra (Figure S2) confirmed the successful formation of CuS-PAAmAN-PEG as the peak for –SH groups disappeared. The resulting product, CuS-PAAmAN-PEG, readily formed a stable CuS-based micelle in an aqueous solution. The average hydrodynamic diameter of CuS-based micelles was 63 nm (PDI = 0.20; Figure 4A). A representative TEM image shown in Figure 4B also demonstrated that CuS-based micelles displayed good dispersity. The average size of dried micelles measured by TEM was 37 nm. This size range of the CuS-based micelles is desirable for targeted cancer therapies.[41,42] The hydrophobic anticancer drug, AF, was encapsulated into the hydrophobic core (i.e., the PAAmAN segment) of the resulting CuS-based micelles via hydrophobic interactions and hydrogen bonding. The AF loading level was determined to be 15.6%.

3.2. Thermoresponsiveness, Photothermal Properties, and NIR-Controlled Drug Release of CuS-Based Micelles

PAAmAN is a unique thermoresponsive polymer that exhibits a UCST in an aqueous solution. The UCST of PAAmAN can be controlled by adjusting the molar ratio of the AAm and AN monomers.[31] In this study, to maintain the micelle structure and avoid premature drug release under normal physiological conditions (i.e., ~37.4 °C), we carefully tuned the molar ratios of AAm/AN to ensure that the phase transition occurred above the body temperature (Figure S3). As shown in Figure 5A, the phase transition of the micelles ([AAm]/[AN] = 6.2/1) induced by temperature started at around 38 °C, which is slightly higher than human body temperature. The phase transition completed at 41 °C, and a clear solution was observed. In addition, the average hydrodynamic diameter of the CuS-based micelles above UCST was increased from 63 nm (at 25 °C) to 81 nm (at 42 °C), (Figure S4), which is attributed to the hydrophobic-to-hydrophilic transition of the PAAmAN segments because the hydrophilic PAAmAN blocks can extend freely into an aqueous solution. Thermoresponsive micelles with a sharp transition window are suitable for targeted cancer therapy because the hydrophobic-to-hydrophilic transition of the micelle core can induce a rapid release of the encapsulated hydrophobic drugs (as detailed below), thus potentially leading to a superior therapeutic efficacy.[32,34]

To evaluate the NIR-induced photothermal effect of the CuS-based micelles, the temperature elevations of the CuS-based micelle solutions at different concentrations were examined upon 980 nm laser irradiation at a power density of 0.75 W/cm^2. Although an 808 nm laser was first used to trigger the photothermal ablation of CuS NPs,[28] recent studies implied that a 980 nm laser may be a better choice due to the higher absorbance of CuS NPs at 980 nm (the absorption peak of CuS NPs in this study was 989 nm).[27,43] As shown in Figure 5B, a clear temperature elevation was observed. As expected, the laser-induced thermal effect is highly dependent on the concentrations of the CuS-based micelles. After 5 min laser irradiation, the temperature elevation of the aqueous solution increased by 7–18 °C with the CuS-based micelle concentration ranging from 6 to 60 μg/mL. These data again indicate that CuS-based NPs can serve as efficient photothermal coupling agents for PTT.

The NIR-triggered temperature elevations of the CuS-based micelle solutions can not only induce photothermal ablation of cells but also cause the phase transition of the micelles, as discussed earlier. In other words, the NIR-triggered temperature elevation of the CuS-based

micelle solution can also cause a hydrophobic-to-hydrophilic transition of the PAAmAN micelle core, thereby enabling NIR-controlled drug release. To validate our hypothesis, the size distribution of the CuS-based micelles after NIR irradiation was measured by DLS (Figure S4). After 10 min NIR irradiation, the hydrodynamic diameter of the CuS-micelles was increased to 79 nm, which is consistent with the temperature-induced size increases once above their UCST. The in vitro drug release profiles were then measured in both PBS (pH 7.4) and acetate buffer (pH 5.3) solutions that mimic the physiological conditions (e.g., the bloodstream, intracellular cytosol, and extracellular space) and acidic endocytotic compartments, respectively. As shown in Figure 5C, without laser irradiation, AF was released in a pH-dependent manner. To be more specific, at a pH of 7.4, only a minimal amount (i.e., ~9%) of AF was released after 48 h, whereas AF was released faster at a pH of 5.3, with 53% of AF being released after 48 h. This pH-dependent manner is likely due to the protonation of the aniline group of the AF molecule under acidic conditions. The resulting salt form of AF has better water solubility and thus can be easily released.[12] However, after 10 min irradiation with a 980 nm laser (i.e., at 6 h), the rates of drug release increased markedly at both pH conditions (about 40% increase within 2 h of laser irradiation). This strongly indicates that the temperature elevation induced by the CuS-based micelles under NIR irradiation successfully caused the hydrophobic-to-hydrophilic transition of the micelles, thus leading to rapid drug release. Notably, we and others have previously demonstrated that a faster drug release within tumors can lead to better therapeutic indexes.[32–35]

3.3. Cellular Uptake Behavior and Cell Viability Tests in a 2D Monolayer Cell Model

EGFR is often overexpressed in many types of cancers, including triple-negative breast cancers.[12] Herein, GE11 peptide, a ligand that can efficiently bind to the EGFR, was conjugated onto the CuS-based micelles to achieve active tumor-targeting capability. The cellular uptake behavior of the Cy5-tagged micelles was first evaluated in a 2D MDA-MB-468 TNBC cell model. Cells were treated with either nontargeted CuS-based micelles, targeted CuS-based micelles, or a combination of targeted CuS-based micelles and free GE11 peptide (i.e., blocking assay). The fluorescence images (Figure 6A) indicate that the intracellular fluorescence of Cy5-tagged targeted CuS-based micelles was significantly stronger than that of Cy5-tagged nontargeted CuS-based micelles. However, when the EGFR on the MDA-MB-468 cells was blocked by an excess amount of free GE11 peptide (i.e., the blocking assay), the cellular uptake of the targeted CuS-based micelles was similar to that of the nontargeted ones. This demonstrates that GE11 conjugation can markedly enhance the cellular uptake of micelles through EGFR-mediated endocytosis. These findings were further verified through quantitative flow cytometry analyses. As shown in Figure 6B, the cellular uptake of targeted CuS-based micelles was nearly 48-fold higher than that of nontargeted ones. Similarly, the blocking assay clearly showed that the cellular uptake of targeted CuS-based micelles in the presence of free GE11 peptide was comparable to that of nontargeted micelles.

The in vitro cell viability tests of various formulations were then carried out. As demonstrated above, CuS-based micelles can effectively convert NIR light energy to heat, which can be utilized for PTT as well as triggering a fast drug release for chemotherapy. In

this experiment, the effects of chemotherapy alone, PTT alone, and combination chemotherapy and PTT were investigated. Various treatment groups are summarized in Table 1. As shown in Figure 6C, empty CuS-based (nontargeted or targeted) micelles without laser illumination did not cause any apparent cytotoxicity. Notably, empty CuS-based micelles themselves did not induce any significant cell death up to 300 μg/mL in both cancer cells and normal cells (WI-38 human lung fibroblast cells) (Figure S5), demonstrating good biocompatibility of the micelles. In contrast, under laser illumination for 10 min, both nontargeted and targeted CuS-based micelles exhibited significant cytotoxicities, with 19 and 37% cell death, respectively, thus demonstrating the effectiveness of PTT. As expected, empty targeted micelles were much more effective at killing cancer cells than empty nontargeted micelles under NIR illumination due to their enhanced cellular uptake through EGFR-mediated endocytosis. Pure AF (an anticancer drug) with and without laser application led to 64 and 61% cell death, respectively, suggesting that the 980 nm laser application did not influence the function of pure AF. For the groups treated with AF-loaded nontargeted and targeted micelles without laser irradiation, 39 and 60% cell deaths were observed, respectively. However, a significant increase in cell deaths was observed when cells treated with either AF-loaded nontargeted (i.e., 58% cell death) or AF-loaded targeted micelles (i.e., 91% cell death) were also subjected to 980 nm laser treatment, demonstrating the superior effect of combination chemotherapy and PTT. Specifically, combination chemotherapy and PTT (AF-loaded targeted micelles under 980 laser irradiation, 91% cell death) provided a dramatically better therapeutic index than that of chemotherapy alone (AF-loaded targeted micelles without laser application, 60% cell death) or PTT alone (empty targeted micelles, 37% cell death). The additive therapeutic efficacy (T_{add}) of pure chemotherapy and PTT, calculated on the basis of the following formula: $T_{add} = 1 - (f_{chemotherapy} \times f_{PTT})$, where f is the cell viability of each treatment,[44–46] was 71%. The measured therapeutic efficacy of combination chemotherapy and PTT (i.e., 91%) was higher than the additive therapeutic efficacy of chemotherapy and PTT (i.e., 71%), demonstrating a synergistic effect for the combination therapy.[44–46] Similarly, the increased cytotoxicity in targeted groups over nontargeted groups was attributed to the enhanced cellular uptake of the targeted micelles, as discussed earlier.

3.4. Micelle Penetration and Cell Viability Tests in a 3D MCTS Model

MCTS has been widely utilized to examine the efficacy of drug delivery systems in vitro. Although MCTSs cannot perfectly mimic in vivo characteristics of tumors as they lack some key features, such as high interstitial pressure, the presence of microvasculature, and the mixture of extracellular matrix and many other cells, they still possess a number of biologically relevant characteristics that bridge 2D monolayer cell models and in vivo models.[47,48] In this study, we developed MDA-MB-468 MCTSs with a size around 500 μm by adopting the mature hanging drop method.[39,40] The micelle penetration behavior was investigated in these MCTSs.

As shown in Figure 7, after 2 h incubation, micelles mostly accumulated on the peripheries of the MCTSs with minimal signals observed inside. The MCTSs treated with targeted (T) micelles showed higher red fluorescence (Cy5 dye) than that from the ones treated with nontargeted (NT) micelles, thus indicating that the targeted micelles efficiently enhanced the

cellular uptake, as demonstrated earlier using the 2D monolayer cell model. However, 6 h postincubation, the targeted micelles penetrated markedly deeper than the nontargeted ones. The MCTSs treated with the targeted micelles showed an obvious micelle distribution inside the tumor spheroids. In contrast, the nontargeted micelles penetrated only slightly deeper and were still limited to the edge of the tumor spheroids. It was previously reported that NPs modified with a targeting ligand can facilitate the penetration of NPs into tumor spheroids.[49–51] Similarly, 24 h postincubation, the nontargeted micelles behaved similarly with a limited penetration depth, whereas the targeted micelles showed a considerably higher and more homogeneous distribution in the central area of the tumor spheroids.

The anticancer efficacies of various formulations were also evaluated in the 3D MCTS model. In the laser treatment groups, cells were treated with various formulations (Table 1) for 6 h before laser application (980 nm; 0.75 W/cm^2; 10 min) and kept for another 18 h. MCTSs treated with the same formulations, but without laser treatment, were also kept for 24 h. The cell viabilities were first determined by a standard MTT assay. As shown in Figure 8A, without laser treatment, neither empty nontargeted nor targeted micelles exhibited any cytotoxicity in MCTSs; on the other hand, empty nontargeted and targeted micelles under 980 nm irradiation showed 14 and 26% cell deaths, respectively, which was caused by the NIR-induced PTT effect. Pure AF showed a significant reduction in cell viability (i.e., ~45% cell deaths), and the laser did not cause any additional cytotoxic effect. The AF-loaded nontargeted and targeted micelles without laser (pure chemotherapy) led to 35 and 52% cell deaths, respectively; however, with laser treatment, enabling combination chemotherapy and PTT, AF-loaded nontargeted and targeted micelles induced 54 and 75% cell deaths, respectively. Overall, the targeted groups outperformed the nontargeted ones, which is consistent with the micelle penetration results as discussed above. More importantly, combination therapy exhibited a significant synergistic effect compared to that of chemotherapy alone or PTT alone, as more cell death (75%, targeted group for example) was observed than T_{add} (65%) of chemotherapy alone (52%) and PTT alone (26%). These results were further confirmed by the PI/annexin-V dead/apoptosis assay. As shown in Figure 8B, a similar observation was made where AF-loaded targeted micelles under NIR irradiation induced the highest cell death (the last bar) with a synergistic therapeutic effect of combination chemotherapy and PTT.

3.5. Photoacoustic Imaging Capability Tests

Photoacoustic (PA) imaging is a noninvasive imaging modality. In PA imaging, optical energy absorbed by light-absorbing tissues or contrasting agents results in a thermoelastic expansion that creates reflected ultrasound signals. Owing to its ability to absorb light in the NIR region, the CuS-based micelle in this study is a desirable contrast agent for PA imaging.[29] As shown in Figure 9A, CuS-based micelles can generate sufficient PA signals. An obvious linear correlation was observed between the micelle concentration and the PA signal (Figure 9B). Notably, most of the previously studied contrast agents for PA imaging (e.g., gold nanostructures, carbon nanotubes, and organic dyes) exhibit their maximum absorption between 560 and 840 nm.[52,53] The absorption peak for the CuS-based NPs is greater than 900 nm, which can translate to a stronger PA signal with a higher signal-to-noise ratio.[54–56]

Therefore, these CuS-based micelles can potentially serve as excellent PA contrast agents for in vivo PA imaging applications.

4. CONCLUSIONS

A tumor-targeted CuS-based theranostic micelle was developed for NIR-controlled combination chemotherapy and PTT, as well as PA imaging. NIR light can effectively elevate the temperature of the CuS-based micelle solution, thereby enabling PTT. Meanwhile, the unique thermoresponsive PAAmAN core of the CuS-based micelle, which exhibited a UCST in an aqueous solution, underwent a hydrophobic-to-hydrophilic transition upon the temperature elevation induced by NIR light irradiation, thereby triggering a rapid drug release and enabling NIR-controlled chemotherapy. In a TNBC model, we have demonstrated that GE11-tagged CuS-based micelles significantly enhanced the cellular uptake as well as the micelle penetration in MCTSs. The tumor-targeted combination chemotherapy and PTT achieved by AF-loaded GE11-conjugated CuS-based micelles under NIR irradiation exhibited a synergistic therapeutic outcome. These CuS-based micelles also offered the capability of PA imaging, which makes them a promising cancer nanotheranostic.

Supplementary Material

Refer to Web version on PubMed Central for supplementary material.

Acknowledgments

This project was financially supported by NIH grants (K25CA166178 and R21CA196653). We also thank Professor Wei Xu for kindly providing us with the GFP-expressing MDA-MB-468 cells.

References

1. Kievit FM, Zhang M. Cancer Nanotheranostics: Improving Imaging and Therapy by Targeted Delivery Across Biological Barriers. Adv Mater. 2011; 23:H217–H247. [PubMed: 21842473]
2. Cheng L, Wang C, Feng L, Yang K, Liu Z. Functional Nanomaterials for Phototherapies of Cancer. Chem Rev. 2014; 114:10869–10939. [PubMed: 25260098]
3. Mehlen P, Puisieux A. Metastasis: A Question of Life or Death. Nat Rev Cancer. 2006; 6:449–458. [PubMed: 16723991]
4. Szakács G, Paterson JK, Ludwig JA, Booth-Genthe C, Gottesman MM. Targeting Multidrug Resistance in Cancer. Nat Rev Drug Discovery. 2006; 5:219–234. [PubMed: 16518375]
5. Cho K, Wang X, Nie S, Shin DM, et al. Therapeutic Nanoparticles For Drug Delivery in Cancer. Clin Cancer Res. 2008; 14:1310–1316. [PubMed: 18316549]
6. Chen H, Zhang W, Zhu G, Xie J, Chen X. Rethinking Cancer Nanotheranostics. Nat Rev Mater. 2017; 2(17024)
7. Jo SD, Ku SH, Won YY, Kim SH, Kwon IC. Targeted Nanotheranostics for Future Personalized Medicine: Recent Progress in Cancer Therapy. Theranostics. 2016; 6:1362–1377. [PubMed: 27375785]
8. Ma Y, Huang J, Song S, Chen H, Zhang Z. Cancer-Targeted Nanotheranostics: Recent Advances and Perspectives. Small. 2016; 12:4936–4954. [PubMed: 27150247]
9. Bartlett DW, Su H, Hildebrandt IJ, Weber WA, Davis ME. Impact of Tumor-Specific Targeting on the Biodistribution and Efficacy of Sirna Nanoparticles Measured by Multimodality in Vivo Imaging. Proc Natl Acad Sci US A. 2007; 104:15549–15554.

10. Chen G, Jaskula-Sztul R, Harrison A, Dammalapati A, Xu W, Cheng Y, Chen H, Gong S. KE108-Conjugated Unimolecular Micelles Loaded with a Novel HDAC Inhibitor Thailandepsin-A for Targeted Neuroendocrine Cancer Therapy. Biomaterials. 2016; 97:22–33. [PubMed: 27156249]
11. Maeda H, Nakamura H, Fang J. The EPR Effect for Macromolecular Drug Delivery to Solid Tumors: Improvement of Tumor Uptake, Lowering Of Systemic Toxicity, and Distinct Tumor Imaging in Vivo. Adv Drug Delivery Rev. 2013; 65:71–79.
12. Brinkman AM, Chen G, Wang Y, Hedman CJ, Sherer NM, Havighurst TC, Gong S, Xu W. Aminoflavone-Loaded EGFR-Targeted Unimolecular Micelle Nanoparticles Exhibit Anti-Cancer Effects In Triple Negative Breast Cancer. Biomaterials. 2016; 101:20–31. [PubMed: 27267625]
13. Zhang P, Hu C, Ran W, Meng J, Yin Q, Li Y. Recent Progress in Light-Triggered Nanotheranostics For Cancer Treatment. Theranostics. 2016; 6:948–968. [PubMed: 27217830]
14. Ganta S, Devalapally H, Shahiwala A, Amiji M. A Review of Stimuli-Responsive Nanocarriers for Drug and Gene Delivery. J Controlled Release. 2008; 126:187–204.
15. Xing Y, Zhao J, Conti PS, Chen K. Radiolabeled Nanoparticles for Multimodality Tumor Imaging. Theranostics. 2014; 4:290–306. [PubMed: 24505237]
16. Li K, Liu B. Polymer-Encapsulated Organic Nanoparticles for Fluorescence and Photoacoustic Imaging. Chem Soc Rev. 2014; 43:6570–6597. [PubMed: 24792930]
17. Chen G, Wang L, Cordie T, Vokoun C, Eliceiri KW, Gong S. Multi-Functional Self-Fluorescent Unimolecular Micelles for Tumor-Targeted Drug Delivery and Bioimaging. Biomaterials. 2015; 47:41–50. [PubMed: 25682159]
18. Chinen AB, Guan CM, Ferrer JR, Barnaby SN, Merkel TJ, Mirkin CA. Nanoparticle Probes for the Detection of Cancer Biomarkers, Cells, and Tissues by Fluorescence. Chem Rev. 2015; 115:10530–10574. [PubMed: 26313138]
19. Guo J, Hong H, Chen G, Shi S, Zheng Q, Zhang Y, Theuer CP, Barnhart TE, Cai W, Gong S. Image-Guided and Tumor-Targeted Drug Delivery with Radiolabeled Unimolecular Micelles. Biomaterials. 2013; 34:8323–8332. [PubMed: 23932288]
20. Li L, Liu T, Fu C, Liu H, Tan L, Meng X. Multifunctional Silica-Based Nanocomposites for Cancer Nanotheranostics. J Biomed Nanotechnol. 2014; 10:1784–1809. [PubMed: 25992441]
21. Zheng M, Yue C, Ma Y, Gong P, Zhao P, Zheng C, Sheng Z, Zhang P, Wang Z, Cai L. Single-Step Assembly of DOX/ICG Loaded Lipid–Polymer Nanoparticles for Highly Effective Chemo-Photothermal Combination Therapy. ACS Nano. 2013; 7:2056–2067. [PubMed: 23413798]
22. Wang C, Xu H, Liang C, Liu Y, Li Z, Yang G, Cheng L, Li Y, Liu Z. Iron Oxide@Polypyrrole Nanoparticles as a Multifunctional Drug Carrier for Remotely Controlled Cancer Therapy with Synergistic Antitumor Effect. ACS Nano. 2013; 7:6782–6795. [PubMed: 23822176]
23. Xu X, Ho W, Zhang X, Bertrand N, Farokhzad O. Cancer Nanomedicine: From Targeted Delivery to Combination Therapy. Trends Mol Med. 2015; 21:223–232. [PubMed: 25656384]
24. Zou L, Wang H, He B, Zeng L, Tan T, Cao H, He X, Zhang Z, Guo S, Li Y. Current Approaches of Photothermal Therapy in Treating Cancer Metastasis with Nanotherapeutics. Theranostics. 2016; 6:762–772. [PubMed: 27162548]
25. Jaque D, Maestro LM, Del Rosal B, Haro-Gonzalez P, Benayas A, Plaza J, Rodriguez EM, Sole JG. Nanoparticles for Photothermal Therapies. Nanoscale. 2014; 6:9494–9530. [PubMed: 25030381]
26. Abadeer NS, Murphy CJ. Recent Progress in Cancer Thermal Therapy Using Gold Nanoparticles. J Phys Chem C. 2016; 120:4691–4716.
27. Chen F, Hong H, Goel S, Graves SA, Orbay H, Ehlerding EB, Shi S, Theuer CP, Nickles RJ, Cai W. In Vivo Tumor Vasculature Targeting of CuS@MSN Based Theranostic Nanomedicine. ACS Nano. 2015; 9:3926–3934. [PubMed: 25843647]
28. Zhou M, Zhang R, Huang M, Lu W, Song S, Melancon MP, Tian M, Liang D, Li C. A Chelator-Free Multifunctional [64Cu] Cus Nanoparticle Platform for Simultaneous Micro-PET/CT Imaging and Photothermal Ablation Therapy. J Am Chem Soc. 2010; 132:15351–15358. [PubMed: 20942456]
29. Ku G, Zhou M, Song S, Huang Q, Hazle J, Li C. Copper Sulfide Nanoparticles as A New Class of Photoacoustic Contrast Agent for Deep Tissue Imaging at 1064 nm. ACS Nano. 2012; 6:7489–7496. [PubMed: 22812694]

30. Xu M, Wang LV. Photoacoustic Imaging in Biomedicine. Rev Sci Instrum. 2006; 77(041101)
31. Seuring J, Agarwal S. First Example of a Universal and Cost-Effective Approach: Polymers with Tunable Upper Critical Solution Temperature in Water and Electrolyte Solution. Macromolecules. 2012; 45:3910–3918.
32. Chen G, Jaskula-Sztul R, Esquibel CR, Lou I, Zheng Q, Dammalapati A, Harrison A, Eliceiri KW, Tang W, Chen H, et al. Neuroendocrine Tumor-Targeted Upconversion Nanoparticle-Based Micelles for Simultaneous NIR-Controlled Combination Chemotherapy and Photodynamic Therapy, and Fluorescence Imaging. Adv Funct Mater. 2017; 27(1604671)
33. Cheng R, Meng F, Deng C, Klok HA, Zhong Z. Dual and Multi-Stimuli Responsive Polymeric Nanoparticles for Programmed Site-Specific Drug Delivery. Biomaterials. 2013; 34:3647–3657. [PubMed: 23415642]
34. Dai J, Lin S, Cheng D, Zou S, Shuai X. Interlayer-Crosslinked Micelle with Partially Hydrated Core Showing Reduction and pH Dual Sensitivity for Pinpointed Intracellular Drug Release. Angew Chem, Int Ed. 2011; 50:9404–9408.
35. Chytil P, Etrych T, Koňák Č, Šírová M, Mrkvan T, Bouček J, Říhová B, Ulbrich K. New HPMA Copolymer-Based Drug Carriers with Covalently Bound Hydrophobic Substituents for Solid Tumour Targeting. J Controlled Release. 2008; 127:121–130.
36. Chen G, Wang Y, Xie R, Gong S. Tumor-Targeted pH/Redox Dual-Sensitive Unimolecular Nanoparticles for Efficient siRNA Delivery. J Controlled Release. 2017; 259:105–114.
37. Boyer C, Liu J, Bulmus V, Davis TP. RAFT Polymer End-Group Modification and Chain Coupling/Conjugation Via Disulfide Bonds. Aust J Chem. 2009; 62:830–847.
38. Dan M, Huo F, Xiao X, Yang S, Zhang W. Temperature-Sensitive Nanoparticle-to-Vesicle Transition of ABC Triblock Copolymer Corona–Shell–Core Nanoparticles Synthesized by Seeded Dispersion RAFT Polymerization. Macromolecules. 2014; 47:1360–1370.
39. Nagelkerke A, Bussink J, Sweep FCGJ, Span PN. Generation of Multicellular Tumor Spheroids Of Breast Cancer Cells: How to Go Three-Dimensional. Anal Biochem. 2013; 437:17–19. [PubMed: 23435308]
40. Ware MJ, Colbert K, Keshishian V, Ho J, Corr SJ, Curley SA, Godin B. Generation of Homogenous Three-Dimensional Pancreatic Cancer Cell Spheroids Using an Improved Hanging Drop Technique. Tissue Eng, Part C. 2016; 22:312–321.
41. Cabral H, Matsumoto Y, Mizuno K, Chen Q, Murakami M, Kimura M, Terada Y, Kano M, Miyazono K, Uesaka M, et al. Accumulation of Sub-100 nm Polymeric Micelles in Poorly Permeable Tumours Depends on Size. Nat Nanotechnol. 2011; 6:815–823. [PubMed: 22020122]
42. Davis ME, Shin DM, et al. Nanoparticle Therapeutics: an Emerging Treatment Modality for Cancer. Nat Rev Drug Discovery. 2008; 7:771–782. [PubMed: 18758474]
43. Tian Q, Tang M, Sun Y, Zou R, Chen Z, Zhu M, Yang S, Wang J, Wang J, Hu J. Hydrophilic Flower-Like CuS Superstructures as an Efficient 980 nm Laser-Driven Photothermal Agent for Ablation of Cancer Cells. Adv Mater. 2011; 23:3542–3547. [PubMed: 21735487]
44. Ma M, Chen H, Chen Y, Wang X, Chen F, Cui X, Shi J. Au Capped Magnetic Core/Mesoporous Silica Shell Nanoparticles for Combined Photothermo-/Chemo-Therapy and Multimodal Imaging. Biomaterials. 2012; 33:989–998. [PubMed: 22027594]
45. Park H, Yang J, Lee J, Haam S, Choi IH, Yoo KH. Multifunctional Nanoparticles for Combined Doxorubicin and Photothermal Treatments. ACS Nano. 2009; 3:2919–2926. [PubMed: 19772302]
46. Hahn GM, Braun J, Har-Kedar I. Thermochemotherapy: Synergism Between Hyperthermia (42–43 degrees) and Adriamycin (of bloom's) in Mammalian Cell Inactivation. Proc Natl Acad Sci US A. 1975; 72:937–940.
47. Pampaloni F, Reynaud EG, Stelzer EH. The Third Dimension Bridges the Gap Between Cell Culture And Live Tissue. Nat Rev Mol Cell Biol. 2007; 8:839–845. [PubMed: 17684528]
48. Shin CS, Kwak B, Han B, Park K. Development of an in Vitro 3D Tumor Model to Study Therapeutic Efficiency of an Anticancer Drug. Mol Pharmaceutics. 2013; 10:2167–2175.
49. Gao H, Xiong Y, Zhang S, Yang Z, Cao S, Jiang X. RGD and Interleukin-13 Peptide Functionalized Nanoparticles for Enhanced Glioblastoma Cells and Neovasculature Dual Targeting Delivery and Elevated Tumor Penetration. Mol Pharmaceutics. 2014; 11:1042–1052.

50. Qin L, Wang CZ, Fan HJ, Zhang CJ, Zhang HW, Lv MH, Cui SD. A Dual-Targeting Liposome Conjugated with Transferrin and Arginine-Glycine-Aspartic Acid Peptide for Glioma-Targeting Therapy. Oncol Lett. 2014; 8:2000–2006. [PubMed: 25289086]

51. Gao H, Yang Z, Zhang S, Pang Z, Liu Q, Jiang X. Study and Evaluation of Mechanisms of Dual Targeting Drug Delivery System with Tumor Microenvironment Assays Compared with Normal Assays. Acta Biomater. 2014; 10:858–867. [PubMed: 24239900]

52. Kim C, Cho EC, Chen J, Song KH, Au L, Favazza C, Zhang Q, Cobley CM, Gao F, Xia Y, et al. In Vivo Molecular Photoacoustic Tomography of Melanomas Targeted by Bio-Conjugated Gold Nanocages. ACS Nano. 2010; 4:4559–4564. [PubMed: 20731439]

53. De La Zerda A, Zavaleta C, Keren S, Vaithilingam S, Bodapati S, Liu Z, Levi J, Smith BR, Ma TJ, Oralkan O, et al. Carbon Nanotubes as Photoacoustic Molecular Imaging Agents in Living Mice. Nat Nanotechnol. 2008; 3:557–562. [PubMed: 18772918]

54. Zhou M, Tian M, Li C. Copper-Based Nanomaterials for Cancer Imaging and Therapy. Bioconjugate Chem. 2016; 27:1188–1199.

55. Santiesteban DY, Dumani DS, Profili D, Emelianov SY. Copper Sulfide Perfluorocarbon Nanodroplets as Clinically Relevant Photoacoustic/Ultrasound Imaging Agents. Nano Lett. 2017; 17:5984–5989. [PubMed: 28926263]

56. Ku G, Zhou M, Song S, Huang Q, Hazle J, Li C. Copper Sulfide Nanoparticles as a New Class Of Photoacoustic Contrast Agent for Deep Tissue Imaging At 1064-nm. ACS Nano. 2012; 6:7489–7496. [PubMed: 22812694]

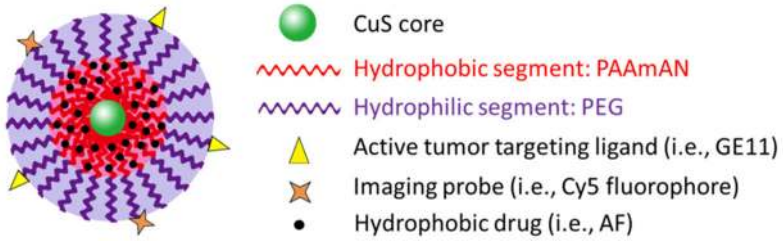

Figure 1.
Schematic illustration of a tumor-targeted CuS-based theranostic micelle.

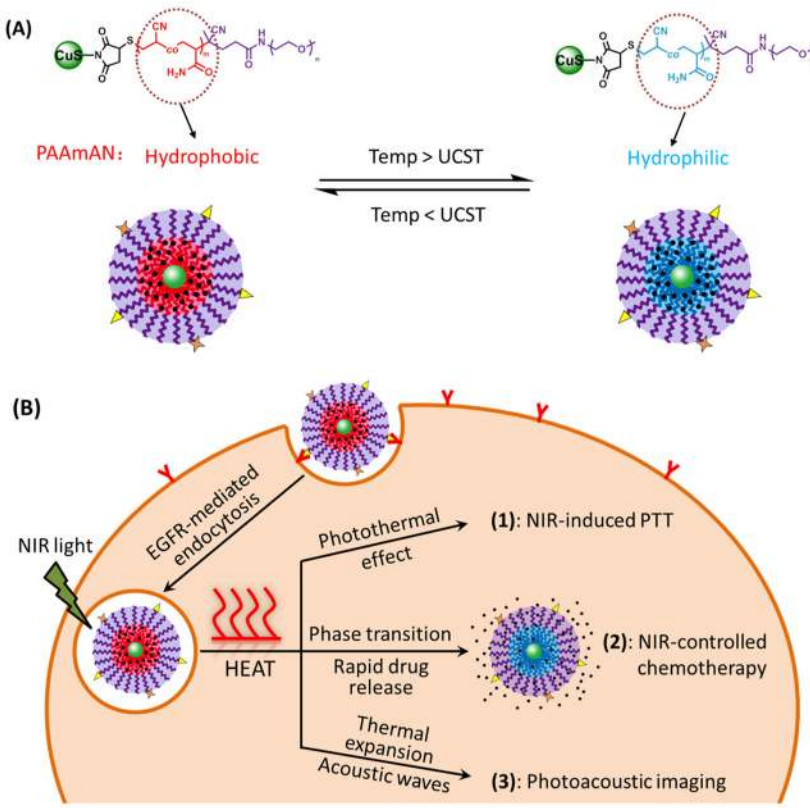

Figure 2.

(A) Illustration of the temperature-induced hydrophobic-to-hydrophilic phase transition of the micelle core formed by PAAmAN segments. (B) Schematic diagram of tumor-targeted CuS-based theranostic micelles for NIR-controlled combination chemotherapy and PTT, as well as photoacoustic imaging.

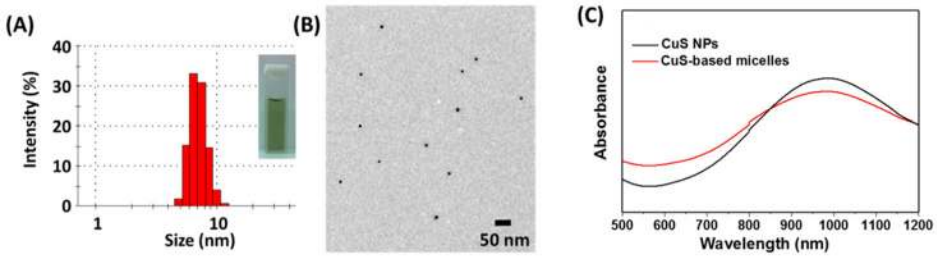

Figure 3.

(A) DLS analysis of CuS-Mal NPs. The inset shows a digital photo of CuS NPs in water. (B) TEM image of CuS-Mal NPs. (C) UV–vis–NIR absorption spectrum of CuS-Mal NPs and CuS-based micelles in water.

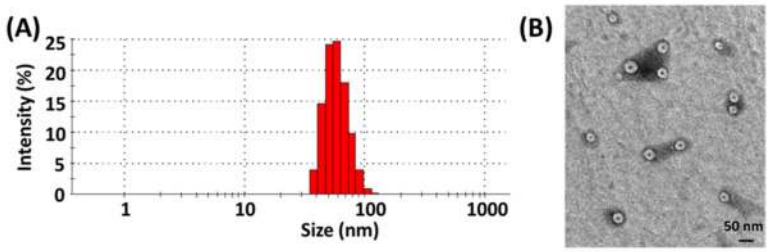

Figure 4.
(A) DLS analysis and (B) TEM image of CuS-based micelles.

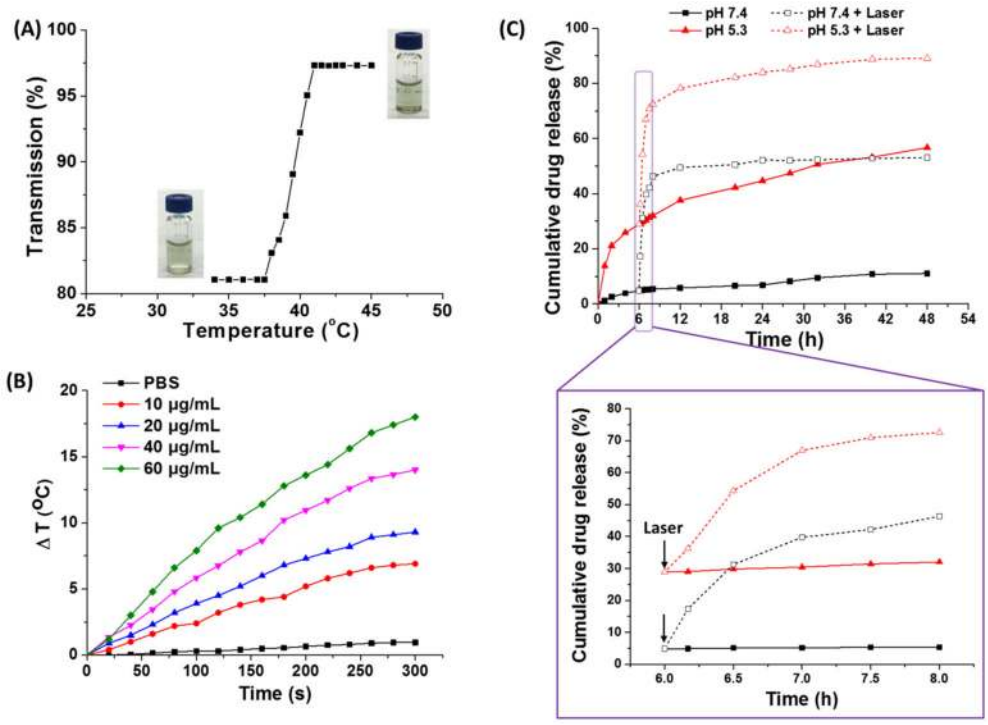

Figure 5.

(A) Temperature–transmission profiles of CuS-based micelles (1 mg/mL). (B) Quantitative temperature changes of CuS-based micelle solutions with different concentrations as a function of 980 nm laser exposure time. (C) NIR-triggered in vitro drug release profile.

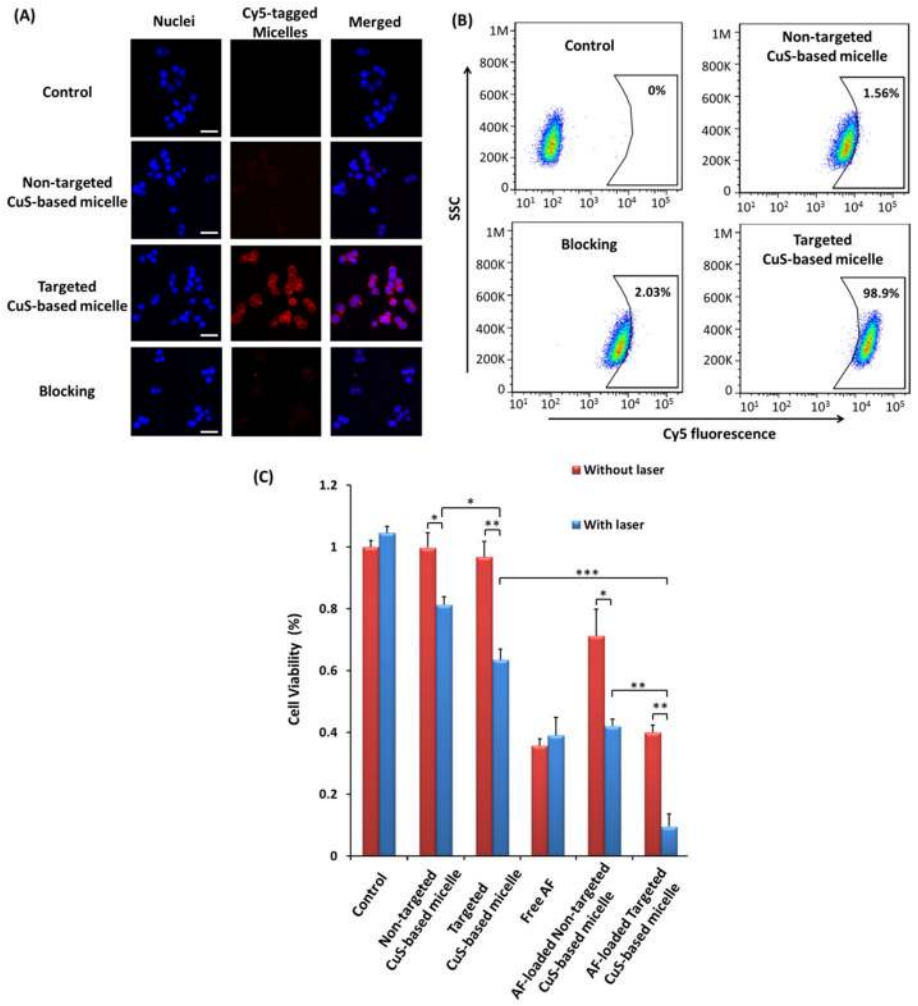

Figure 6.

In vitro cellular uptake studies using (A) fluorescence microscopy and (B) flow cytometry. MDA-MB-468 cells were treated with complete medium (i.e., control), nontargeted CuS-based micelles, targeted CuS-based micelles, and a combination of targeted CuS-based micelles and free GE11 peptide (i.e., blocking; 2 μM) at a micelle concentration of 100 μg/mL for 2 h. Scale bar: 50 μm. (C) Cell viability tests using an MTT assay in a 2D monolayer cell model. Cells were treated with various formulations as summarized in Table 1 with an AF concentration of 0.05 μg/mL. For laser-related treatments, cells were irradiated by a 980 nm laser (0.75 W/cm^2, 10 min) after 6 h incubation of micelles. Data are displayed as a mean ± standard deviation (SD) ($n = 5$). *: $p < 0.05$; **: $p < 0.01$; ***: $p < 0.001$.

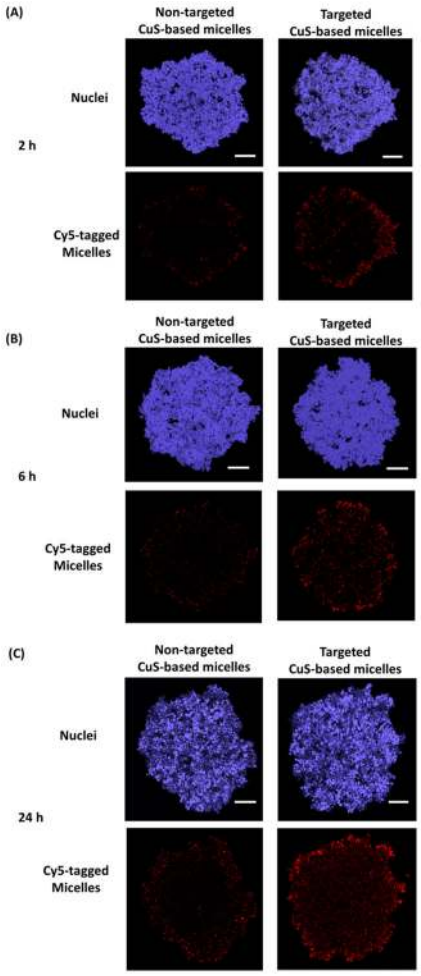

Figure 7.

Micelle penetration studies in a 3D MCTS model. MDA-MB-468 cell spheroids were treated with Cy5-tagged nontargeted and targeted CuS-based micelles for (A) 2 h, (B) 6 h, and (C) 24 h at a micelle concentration of 100 μg/mL. Scale bar: 100 μm.

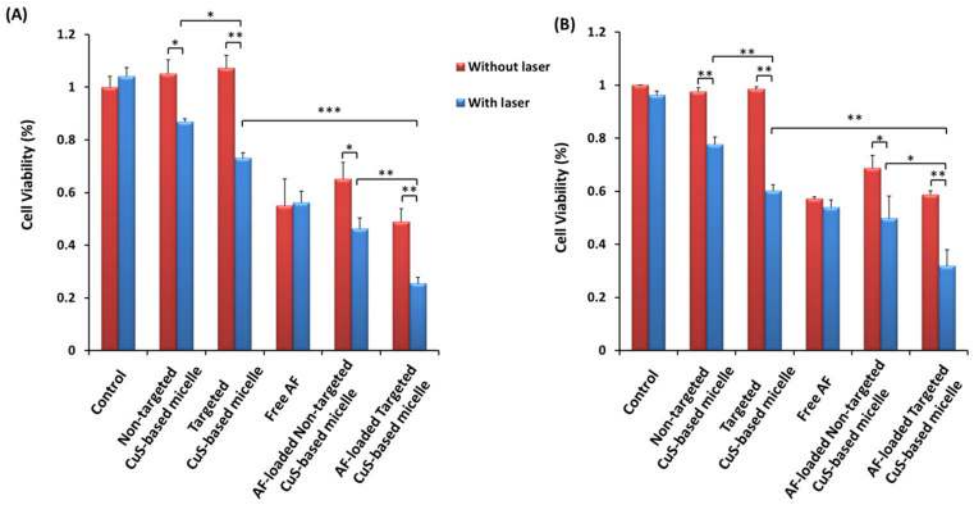

Figure 8.

Cell viability studies using a 3D MCTS model. (A) MTT assay and (B) PI/annexin-V dead/apoptosis assay. MCTSs were treated with various formulations as summarized in Table 1 with an AF concentration of 0.05 μg/mL. For laser-related treatments, MCTSs were irradiated by a 980 nm laser (0.75 W/cm^2, 10 min) after 6 h incubation of micelles. Values were presented as a mean ± SD (n = 3). *: $p < 0.05$; **: $p < 0.01$; ***: $p < 0.001$.

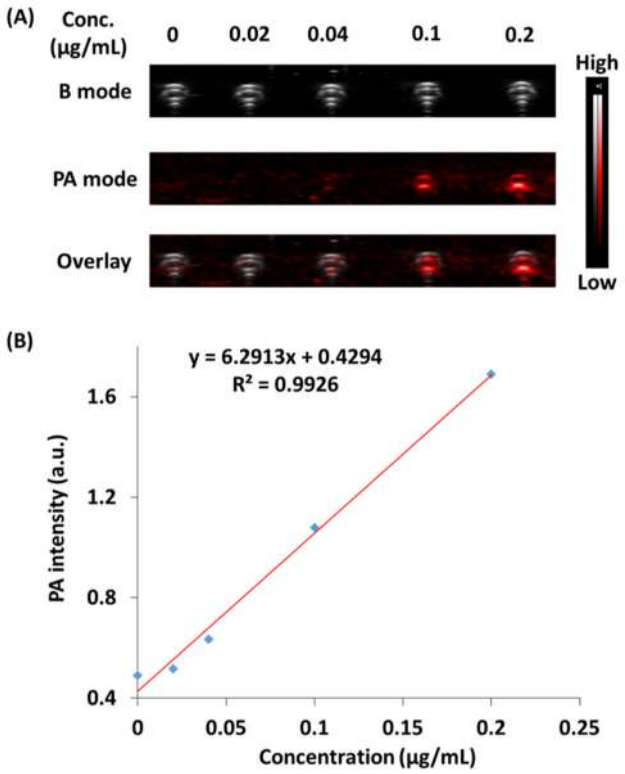

Figure 9.

(A) PA imaging of CuS-based micelles at various micelle concentrations. (B) Linear correlation of the PA intensity of CuS-based micelles against their corresponding concentrations.

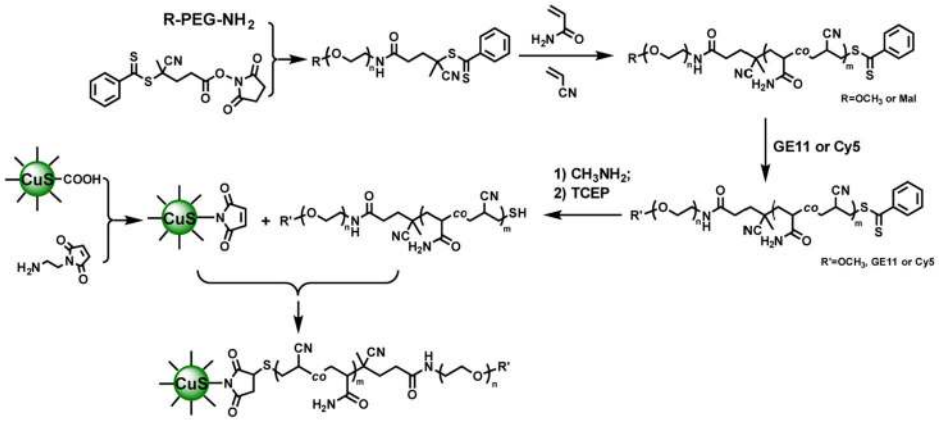

Scheme 1.

Synthetic Scheme of CuS-PAAmAN-PEG-GE11/Cy5/OCH_3, Which Can Form a CuS-Based Micelle in an Aqueous Solution

Table 1

Summary of Various Conditions for the Cell Viability Tests

	without laser	with laser
1	Pure medium (control)	pure medium (control)
2	empty nontargeted CuS-based micelles	empty nontargeted CuS-based micelles
3	empty targeted CuS-based micelles	empty targeted CuS-based micelles
4	AF	AF
5	AF-loaded nontargeted CuS-based micelles	AF-loaded nontargeted CuS-based micelles
6	AF-loaded targeted CuS-based micelles	AF-loaded targeted CuS-based micelles